

1 **The effects of turbulent collision-coalescence on**
2 **precipitation formation and precipitation-dynamical**
3 **feedbacks in simulations of stratocumulus and shallow**
4 **cumulus convection**

5
6 **Charmaine N. Franklin**^{1,2}

7 [1]{CSIRO Marine and Atmospheric Research, Aspendale, Victoria, Australia}

8 [2]{Centre for Australian Weather and Climate Research, A partnership between CSIRO and
9 the Australian Bureau of Meteorology, Aspendale, Victoria, Australia}

10 Correspondence to: C. N. Franklin (charmaine.franklin@csiro.au)

11
12 **Abstract**

13 A double moment warm rain scheme that includes the effects of turbulence on droplet
14 collision rates has been implemented in a large-eddy model to investigate the impact of
15 turbulence effects on clouds and precipitation. Simulations of shallow cumulus and
16 stratocumulus show that different precipitation-dynamical feedbacks occur in these regimes
17 when the effects of turbulence are included in the microphysical processes. In both cases
18 inclusion of turbulent microphysics increases precipitation due to a more rapid conversion of
19 cloud water to rain. In the shallow convection case, the greater water loading in the upper
20 cloud levels reduces the buoyancy production of turbulent kinetic energy and the entrainment.
21 The stratocumulus case on the other hand shows a weak positive precipitation feedback, with
22 enhanced rainwater producing greater evaporation, stronger circulations and more turbulence.
23 Sensitivity studies where the cloud droplet number was varied show that greater number
24 concentrations suppress the stratocumulus precipitation leading to larger liquid water paths.
25 This positive second indirect aerosol effect shows no sensitivity to whether or not the effects
26 of turbulence on droplet collision rates are included. While the sign of the second indirect
27 effect is negative in the shallow convection case whether the effects of turbulence are
28 considered or not, the magnitude of the effect is doubled when the turbulent microphysics are
29 used. It is found that for these two different cloud regimes turbulence has a larger effect than

1 cloud droplet number and the use of a different bulk microphysics schemes on producing
2 rainfall in shallow cumuli. However, for the stratocumulus case examined here, the effects of
3 turbulence on rainfall are not statistically significant and instead it is the cloud droplet number
4 concentration or the choice of bulk microphysics scheme that has the largest control on the
5 rain water.

6

7 **1 Introduction**

8 Cloud microphysical parameterisations are required in atmospheric models of all scales from
9 large-eddy simulation models through to climate models. Correctly representing
10 microphysical processes in models is challenging yet imperative for quantitative precipitation
11 forecasting and climate studies. To enable greater confidence in climate projections one of the
12 processes that requires a quantitative analysis is the second aerosol indirect effect, which is
13 the effect from enhanced aerosol concentrations in clouds suppressing drizzle and prolonging
14 cloud lifetimes (Albrecht 1989). To be able to quantify this effect with any real certainty, the
15 cloud microphysical processes must be accurately represented in global climate models
16 (GCMs), in particular the autoconversion process, which describes the collision and
17 coalescence of small droplets to form larger rain drops.

18 In clouds where the temperature does not reach freezing, it is the process of collision and
19 coalescence that allows drops to grow to a size large enough to fall out of a cloud as rain.
20 Observations of droplet growth tend to show a faster evolution and broader drop size
21 distribution compared to the theoretically calculated drop spectra, where the equations are
22 applied to a randomly distributed population of drops whose motion is governed by
23 gravitational forcing (see review by Grabowski and Wang 2013). Several physical effects
24 have been suggested to play an important role in the reduction of the growth times, including
25 entrainment and mixing of dry air, turbulence and the role of giant cloud condensation nuclei
26 (e.g. Beard and Ochs 1993). Turbulence increases the collision rate of droplets in at least three
27 ways: by changing the droplet velocities and the spatial distribution of the droplets (e.g.
28 Franklin et al. 2005), and by changing the collision and coalescence efficiencies between
29 droplets. Although the effect of turbulence on cloud droplet collision-coalescence rates is yet
30 to be quantified by observations, modelling studies have shown that turbulence can increase
31 the collision rates of droplets by several times the purely gravitational rate (Franklin et al.
32 2005, 2007; Wang et al. 2005; Pinsky et al. 2006).

1 Franklin et al. (2007) performed direct numerical simulations (DNS) of droplets within
2 turbulent flow fields and developed empirically derived equations that describe the turbulent
3 collision kernel for droplet pairs, where the larger droplet is within the radius range of 10 – 30
4 μm and the eddy dissipation rate of turbulent kinetic energy (TKE) is between 100 and 1500
5 $\text{cm}^2 \text{s}^{-3}$. The collision kernels from Franklin et al. (2007) were shown to be in good agreement
6 with those of Kunnen et al. (2013), who used a novel technique to simulate the turbulent flow
7 field in their DNS. These turbulent collision kernels were used in solutions of the stochastic
8 collection equation (SCE) by Franklin (2008) to develop empirical double-moment
9 parameterisations of the effect of autoconversion, accretion and self-collection on the rain and
10 cloud water mixing ratios and the rain and cloud drop number concentrations.
11 Parameterisations using both turbulent and non-turbulent collision kernels were developed.
12 The SCE was solved for liquid water contents in the range of $0.01 - 2 \text{ g kg}^{-1}$, cloud droplet
13 number concentrations up to $500 \text{ drops cm}^{-3}$ and relative dispersion coefficients of the initial
14 drop size distribution between 0.25 and 0.4. The initial drop size distribution was a Gamma
15 function and the separation radius that determined the point at which a cloud droplet becomes
16 a raindrop was $40 \mu\text{m}$. Using the SCE results for such a broad range of drop size distributions
17 gives the resulting parameterisations greater statistical meaning and applicability. The two
18 suites of warm rain parameterisations, turbulent and non-turbulent, allow the investigation of
19 the effect of turbulence on the microphysical processes and the resulting feedbacks in
20 atmospheric models. These effects are explored in this work for stratocumulus and shallow
21 cumulus convection cases. Section 2 describes the model and the two cases to be examined.
22 Section 3 presents the results for the simulated cloud and dynamical structures and Section 4
23 shows the sensitivity of the results to changes in cloud droplet number concentrations. This is
24 followed by a summary of the findings in Section 5.

25

26 **2 Experiment design**

27 The double-moment warm rain microphysics parameterisations of Franklin (2008) have been
28 implemented in the University of California Los Angeles Large Eddy Simulation (UCLA-
29 LES) model. The anelastic LES code is described in Stevens et al. (2005) and solves
30 prognostic equations for the three velocity components, the total water mixing ratio, the liquid
31 water potential temperature and the mass and number concentration of rain. Time integration
32 of the momentum equations uses a leapfrog scheme and scalars are advanced using a forward-

1 in-time method. Advection of the velocity components is solved using fourth-order centred
 2 differences and scalars are advected using a higher order upwind scheme with slope limiting
 3 using a monotone centred method. Subgrid fluxes are modelled using the Smagorinsky-Lilly
 4 model. The mass of cloud water is defined implicitly due to the dependence of the liquid
 5 water potential temperature on the total condensate, and the cloud droplet number
 6 concentration is a fixed parameter. The numerical solution of the cloud processes, including
 7 droplet sedimentation, is described in Savic-Jovicic and Stevens (2008), except that in this
 8 work the separation threshold radius for cloud and rain is taken to be the default values of 40
 9 microns for the schemes of Seifert and Beheng (2001) and Franklin (2008), and 25 microns
 10 for Khairoutdinov and Kogan (2000).

11 In this work the cloud droplet number concentration (CDNC) is constant. Observations of the
 12 shallow cumulus case described in Section 2.1 show an approximately constant droplet
 13 concentration with height (vanZanten et al. 2011). Slawinska et al. (2012) demonstrated the
 14 reason behind the observed constant CDNC being due to significant in-cloud activation of
 15 cloud condensation nuclei. Using a bin microphysics LES, Wyszogrodzki et al. (2013)
 16 showed that while CDNC were constant with height for the majority of occurrences in their
 17 simulations, there is variability in the CDNC fields. Therefore, while the use of a constant
 18 CDNC is a good assumption, variations in CDNC will likely affect the development of
 19 precipitation and this will not be captured in the simulations presented in this work.

20 The default bulk microphysics scheme in the UCLA-LES is that of Seifert and Beheng
 21 (2001). In this study the autoconversion and accretion parameterisations of Franklin (2008)
 22 are the main subject of investigation, however, results from the default scheme and that of
 23 Khairoutdinov and Kogan (2000) are also used to give some indication of the range of results
 24 from different microphysics schemes. The turbulent autoconversion equation of Franklin
 25 (2008) has been modified to the following form, which gives a better representation of the
 26 DNS data at higher cloud water contents,

$$\begin{aligned}
 \frac{\partial q_r}{\partial t} \Big|_{auto} &= 2.0026 \times 10^3 \tan\left(-5.2 \times 10^{-2} R_\lambda + 15.78\right) \\
 q_c &^{97.45(-8.4 \times 10^{-1})^{R_\lambda^2} + 2.5} N_c \Big/ \left(-9.0 \times 10^{-1} + 1.28 \times 10^{-2} R_\lambda - 2.3 \times 10^{-4} R_\lambda^2\right)
 \end{aligned}
 \tag{1}$$

28 where q_r and q_c are the rain and cloud water contents (kg m^{-3}), N_c is the cloud droplet
 29 concentration (cm^{-3}) and R_λ is the Taylor microscale Reynolds number of the flow field. This

1 expression will underestimate the effects of turbulence on droplet collision-coalescence due to
2 the use of gravitational collision efficiencies. Limited data are available for the effects of
3 turbulence on collision efficiencies. Currently the DNS data available only provide two data
4 points, for dissipation rates of 100 and 400 cm^2s^{-3} (Wang et al. 2008). To include the turbulent
5 collision efficiencies in this work would require them to be extrapolated out to dissipation
6 rates of 1500 cm^2s^{-3} . The collision kernel results show that the effects of turbulence do not
7 scale linearly with dissipation rate (Franklin et al. 2007) and two data points does not provide
8 enough information to represent this process with any certainty for the high dissipation rates.
9 Therefore, the decision was made not to include the turbulent collision efficiencies until more
10 DNS data become available.

11 In the implementation of the parameterisations of Franklin (2008) and (1), equation (4) of
12 Franklin (2008) has been used to eliminate the dependence on R_λ and make the dependence
13 solely a function of the dissipation rate of TKE. The parameterisations of Franklin (2008)
14 only consider the effects of turbulence on small collector cloud droplets with radii between 10
15 and 30 microns. For these small droplets it is the dissipation range turbulence that governs the
16 droplet motion (e.g. Wang and Maxey 1993) and, therefore, the dissipation rate is the
17 dominant flow property that determines the collision rate, with the Reynolds number effect of
18 significantly less importance. This is illustrated in Figure 4 of Ayala et al. (2008) who show
19 that R_λ effects are only apparent for droplets of radius 40 microns and larger, which are larger
20 than the size of droplets considered in Franklin (2008). This result is also described in
21 Wyszogrodzki et al. (2013) who state that small drops with radius less than 30 microns are
22 not affected by the root mean square velocity, which is the R_λ dependence. This is the
23 reasoning behind the parameterisations of Franklin (2008) and (1) being a function of the
24 dissipation rate only. The DNS simulations used as the basis for this work covered a much
25 wider range of dissipation rates applicable for cloud conditions than other studies, ranging
26 from 100 up to 1500 $\text{cm}^2 \text{s}^{-3}$.

27 As is the approach in Seifert et al. (2010), in the LES implementation of the microphysics
28 scheme R_λ is calculated from the gridbox mean dissipation rate of TKE. Wyszogrodzki et al.
29 (2013) showed that neglecting LES subgrid scale effects on the turbulent enhancement of the
30 gravitational kernel is a reasonable approximation given the current state of knowledge. The
31 autoconversion parameterisation (1) and the implementation described was used by Wang et
32 al. (2013), where this equation and method was shown to produce cloud droplet and rain drop

1 number concentrations and mixing ratios that were in better agreement with observations
2 compared to other autoconversion schemes.

3 **2.1 Description of the shallow convection case - RICO**

4 The initial and boundary conditions and large scale forcings are taken from the Global Energy
5 and Water Experiment (GEWEX) Cloud Systems Study (GCSS) Boundary Layer Cloud
6 Working Group (BLCWG) intercomparison case described by vanZanten et al. (2011). This is
7 a composite case based on observations taken during an undisturbed period of the Rain in
8 Cumulus over the Ocean (RICO) field study (Rauber et al. 2007), which sampled
9 precipitating trade wind cumulus. The domain size of these experiments is 13.2 km square
10 and 5 km deep, with grid spacing of 100 m in the horizontal and 40 m in the vertical. The time
11 step is variable and is chosen as to keep the Courant number between 0.65 and 0.85. The
12 average observed cloud droplet number concentration during RICO was 70 cm^{-3} , and that
13 number has been used for the control simulations. The length of the simulations for this case
14 are 24 hours and the profile statistics are taken as averages over the last 4 hours. After the
15 initial spin up, the model produces numerous shallow precipitating convective clouds as
16 shown in Figure 1a. The clouds typically extend up to 2400 m, have cloud bases at around
17 600 m and tend to be 1-2 km in horizontal extent (Fig. 1b).

18 **2.2 Description of the stratocumulus case – RF02 of DYCOMS II**

19 This case is based on the aircraft measurements taken during the second research flight
20 (RF02) of the second Dynamics and Chemistry of Marine Stratocumulus (DYCOMS II) field
21 campaign (vanZanten and Stevens 2005). The initial conditions and large-scale forcings are
22 taken from the GCSS BLCWG intercomparison study documented by Ackerman et al. (2009).
23 RF02 penetrated nocturnal stratocumulus under a dry inversion consisting of heavy drizzling
24 open cellular convection, as well as lightly drizzling closed cells. The initial conditions are an
25 average over the two cloud populations sampled, except for the cloud droplet number
26 concentration which is the average over the open cells only and set to 55 cm^{-3} . The horizontal
27 domain and grid spacing for this case study are 6.6 km square and 50 m respectively, while
28 the vertical domain is 2 km and the grid spacing varies from 5 m at the surface and the
29 inversion to 80 m at the model top. The model is run for 6 hours and the profile statistics are
30 calculated over the final 4 hours. Typical liquid and rain water cross sections are shown in

1 Figure 2. Maximum liquid water contents occur at cloud top and precipitation reaches the
2 surface.

3 **3 Simulated cloud and dynamical structure**

4 **3.1 Shallow cumulus convection - RICO**

5 The turbulent microphysics parameterisations are applied in the regions of the clouds where
6 the dissipation rates of TKE are between 100 and 1500 $\text{cm}^2 \text{s}^{-3}$, with the higher dissipation
7 rates associated with faster conversion rates from cloud to rain water (Franklin 2008). In the
8 RICO case the range of dissipation rates for which the turbulent microphysics scheme is valid
9 is encountered in extensive regions of the clouds, with the highest dissipation rates occurring
10 near the cloud tops (see Fig. 1b). These increased autoconversion, accretion and self-
11 collection rates increase the rain water mixing ratio of the clouds as compared to the
12 simulation where the non-turbulent parameterisation is used as shown in Figure 3. The results
13 using the well known Seifert and Beheng (2001; SB) scheme are included as a measure of
14 confidence for the more recent schemes of Franklin (2008), and to give some indication as to
15 the uncertainties due to different bulk scheme parameterisations. However, the main focus is
16 on the differences between the turbulent and non-turbulent microphysics schemes that have
17 been derived using the same framework.

18 The rain water mixing ratios are significantly increased when the turbulent microphysics
19 effects are included, with the largest difference occurring at the surface where the turbulent
20 case produces 6 times more rain than the non-turbulent case and 1.5 times more than the
21 simulation with the SB microphysics scheme. While there is a large amount of temporal
22 variability in the rain water profiles as shown by the standard deviations in Figure 3d, the
23 comparison between the simulations with the turbulent and non-turbulent microphysics
24 schemes show a statistically significant increase in the rain water throughout all levels except
25 the uppermost 500 m. The surface area experiencing rainfall increases by a factor of 3, and
26 the rain fraction is also larger throughout the cloud layer in the turbulent microphysics case as
27 compared to the non-turbulent microphysics simulation. The SB simulation produces 1.5
28 times less raining surface area than the turbulent microphysics simulation and the profile of
29 the rain area fraction in the SB simulation shows a different structure to the other simulations.
30 The two Franklin scheme simulations produce larger increases in the rain fractions with
31 height and demonstrate that the inclusion of turbulence effects on the droplet collision rates

1 has less effect on the rain fraction profile than the parameterisation uncertainties associated
2 with bulk schemes. The profiles of liquid water potential temperature and total water mixing
3 ratio show that the largest difference between the cases occurs near the height of the
4 inversion, with the turbulent microphysics simulation being 0.2 K warmer than the case with
5 the non-turbulent microphysics (Fig. 3). The largest difference in cloud fraction occurs in the
6 levels above 1000 m, where more cloud water in the turbulent case generates greater cloud
7 fractions. The simulation using the turbulent microphysics parameterisation has on average
8 greater cloud water throughout the cloud, however, the percentage increase in the amount of
9 rain water produced in this simulation compared to the case using the non-turbulent
10 microphysics is far more than the increase in the cloud liquid water contents and the
11 variability is such that the mean cloud water contents of all the simulations lie within one
12 standard deviation of the mean for the turbulent case.

13 Quantitatively these results are in agreement with the RICO LES simulations of Seifert et al.
14 (2010) who used a different turbulent collision kernel based on the results of Ayala et al.
15 (2008) and Wang et al. (2008). Wyszogrodzki et al. (2013) used the Ayala et al. (2008) kernel
16 in a bin microphysics scheme to simulate a shallow convection case from the Barbados
17 Oceanographic and Meteorological Experiment (BOMEX). Their LES results show increases
18 of accumulated surface precipitation of between 4 and 12 times depending on the cloud
19 condensation nuclei concentration. Together with the results of this study, all these cases have
20 demonstrated that including the effects of turbulence on the droplet collision rates makes a
21 significant difference to the amount of rain that shallow convective clouds produce. As
22 discussed in both of the aforementioned publications, the resolution of these simulations is not
23 fine enough to resolve the structure of these clouds. Seifert et al. (2010) tested the sensitivity
24 of their results to a doubling in horizontal resolution and found a substantial reduction in the
25 surface rain rate; however, the turbulence case still produced significantly greater rain.

26 Time series of the evolution of the liquid water path, rain water path and cloud fractions are
27 shown in Figure 4. There is a spike during the first hour as the initial cloud field develops, and
28 after about 2 hours the cloud cover reaches 12%. The simulation with the turbulent
29 microphysics shows a greater rain water path than the simulation with the non-turbulent
30 microphysics at almost all times of the 24 hour simulations, with a few significant peaks
31 occurring during the last 4 hours. The precipitation intermittency is due to the limited domain
32 size that will only allow for one large rain event at a time (Seifert and Heus 2013). All

1 simulations show similar variability in the cloud fraction, however the average liquid water
2 path variance over the last 4 hours is almost double in the turbulent microphysics simulation.

3 Figure 5 shows that the evaporation of rain water is greatly enhanced in the turbulent
4 microphysics simulation and this is due to an increase in both rain water and rain drop number
5 concentration. The average TKE from the simulation using the turbulent microphysics is less
6 than that of the non-turbulent case in the cloud levels above 2 km, however, in the lower
7 levels including below cloud base, the TKE from the turbulent case is greater than the non-
8 turbulent case. The increased TKE in the subcloud layer of the simulation that includes the
9 turbulence effects on droplet collisions reflects the greater horizontal variability associated
10 with the enhanced evaporation of precipitation destabilising the levels below the cloud (Fig.
11 5d). In the turbulent microphysics simulation the reduced TKE in the upper regions of the
12 cloud is caused by a reduction in the buoyancy production of TKE (Fig. 5c). In this case there
13 is an increase in water loading associated with the increased cloud and rain water, particularly
14 in these upper levels. This increase in water loading reduces the buoyancy production of TKE
15 (Fig. 5c) and reduces the amount of TKE that is transported to the inversion layer that is
16 required for entrainment (Jiang and Cotton 2000).

17 The reduced buoyancy production of TKE in the upper levels of the cloud in the turbulent
18 case is associated with a reduction in the variance of the vertical motion (Fig. 5e). The
19 updrafts within the clouds in the turbulent case are stronger in the upper levels due to the
20 increased latent heating associated with the larger generation of cloud liquid water. This is
21 also reflected in the more positive values of the third moment of vertical velocity in the
22 turbulent microphysics case, indicating smaller, more intense updrafts and larger weaker
23 downdrafts (not shown). These stronger in-cloud vertical velocities occur above the height of
24 the maximum theta gradient (2321 m in the non-turbulent case and 2328 m in the turbulent
25 microphysics case) and reflect the stronger overshooting convection in the turbulent case.

26 Wyszogrodzki et al. (2013) argued that the use of turbulent collision kernels produces a
27 dynamical enhancement to the amount of precipitation generated due to the off-loading of
28 condensed water, which in turn increases buoyancy and cloud top heights. In our case the
29 water loading reduces the buoyancy in the upper levels of the cloud but increases the
30 buoyancy below about 1800 m. Jiang and Cotton (2000) examined the differences between
31 drizzling and non-drizzling shallow convective clouds and also found a reduction in buoyancy
32 and turbulence in their case with larger precipitation.

1 To further examine the buoyancy characteristics of the clouds and estimate the entrainment
2 rates, the conditional averages of vertical velocity, total and liquid water contents within
3 cloud cores are analysed. Cloud cores are defined as the cloudy regions that have positive
4 buoyancy as compared to the slab average. Figure 6a shows that the simulation with the
5 turbulent microphysics has a larger area of cloud cores throughout the mid and upper cloud
6 levels as compared to the simulation with the non-turbulent microphysics. However,
7 comparing these profiles to Fig. 3e, we see that the turbulent microphysics case has a smaller
8 proportion of positively buoyant cloud regions in the levels above 1300 m. The average
9 vertical velocities in the cloud core are very similar in the simulations with the non-turbulent
10 and turbulent microphysics schemes, with the turbulent case having slightly weaker updrafts
11 in the upper cloud core levels. This result together with the vertical velocities averaged over
12 all cloudy regions shown in Figure 5f, shows that the turbulent microphysics simulation has
13 increased vertical velocities in the cloudy regions that are not positively buoyant. This
14 demonstrates that in this simulation it is not the reduced water loading associated with greater
15 precipitation that acts to increase the buoyancy and hence the vertical velocities. Figure 6c
16 shows that the turbulent microphysics simulation has larger average total water contents in the
17 cloud core upper levels and this applies to the cloud liquid water as well (Fig. 6d). Diagnosing
18 the mass flux and fractional entrainment rates using equations 11 and 16 of Stevens et al.
19 (2001) and the total moisture mixing ratio, shows that the mass flux in the upper levels is
20 larger for the turbulent microphysics simulation (Fig. 6e) and this is due to the greater area of
21 the cloud cores in this case. The turbulent microphysics simulation has a smaller entrainment
22 rate throughout the vertical compared to the simulation with the non-turbulent microphysics
23 parameterisations, in agreement with the larger water contents in the simulation that includes
24 the effects of turbulence on the droplet collision rates. Note that the application of the mass
25 flux approach with a simple entraining plume model breaks down in the inversion at about 2
26 km (Siebesma et al. 2003) and explains the sharp gradient in Figure 6f.

27 The effect of the dynamical feedback in the RICO case presented here is a negative feedback
28 on the turbulent enhancement of rain water generation. The reduced buoyancy production of
29 TKE in the upper cloud levels where most of the liquid water is located (Figs. 1 and 3),
30 reduces the TKE and dissipation rate of TKE compared to the simulation with the non-
31 turbulent microphysics. Given that the turbulent enhancement is a function of the dissipation
32 rate of TKE, the use of the turbulent microphysics parameterisations acts to reduce the
33 dissipation rate in the cloud levels where the liquid water contents are largest and hence

1 produces a negative feedback. It should be recognised that there is still a significant
2 enhancement of rain water compared to the non-turbulent case and the increased cloud depths
3 discussed by Wyszogrodzki et al. (2013) are present in our simulations. Maximum cloud top
4 heights are larger in the turbulent microphysics simulation compared to the non-turbulent; on
5 average the highest cloud top is 2656 m compared to 2620 m. However, in this case the
6 impact of the enhanced cloud and rain water acts to reduce the TKE rather than promote
7 larger buoyancy production of TKE.

8 The effect of this negative feedback can be seen in Figure 7 where the dissipation rates of
9 TKE are shown for the control simulations and sensitivity tests where the cloud droplet
10 number concentration was reduced from 70 to 40 cm^{-3} . In the simulations with the reduced
11 number concentration the amount of rain water is increased from the control, with the average
12 rain water path in the non-turbulent microphysics simulations increasing from 1.9 to 4.3 g m^{-1}
13 2 , and 7.9 to 10.6 g m^{-2} for the turbulent microphysics simulations. Figure 6 shows the reason
14 why the percentage increase in rain water path is larger for the non-turbulent microphysics
15 case, and this is due to a reduction in the dissipation rate of TKE in the turbulent microphysics
16 simulations due to the negative feedback from the buoyancy generation of TKE, which limits
17 the enhancement from the turbulent microphysics as the rain and cloud water increase.

18 **3.2 Stratocumulus – RF02 of DYCOMS II**

19 Similar to the shallow convection case, the dissipation rates of TKE that affect the
20 microphysics are maximum in the upper levels of the stratocumulus cloud layer; however, for
21 this case the dissipation rates are much weaker (Fig. 2). There are only small regions at the
22 top of the cloud where the dissipation rate reaches $100 \text{ cm}^2 \text{ s}^{-3}$ and, therefore, where the
23 conversion rates between cloud and rain water will be accelerated by turbulence effects in the
24 simulation that uses the turbulent microphysics. These small regions though do make a
25 difference to the precipitation flux and the rain drop number concentration in the cloud and
26 subcloud layers, while the cloud fractions remain relatively unchanged (Fig. 8). The average
27 rainwater path increases by 17% when the turbulent microphysics parameterisations are used;
28 however, the variability is such that this is not a statistically significant result. For this case
29 the microphysics scheme of Khairoutdinov and Kogan (2000; KK) has been used as a
30 comparison for the new schemes, since this scheme was developed specifically for
31 stratocumulus clouds.

1 For this lightly drizzling case the precipitation flux is maximum at cloud top (Fig. 8). The
2 increased rain water in the turbulent microphysics simulation is associated with a greater
3 number of rain drops and larger evaporation rates of rain water, particularly just below cloud
4 base (Figure 9a). The precipitation from the KK scheme does not reach the surface in this case
5 and has a reduced precipitation flux at all levels compared to the schemes of Franklin. Figures
6 8f and 9a show that the rain number concentration is larger in the KK simulations throughout
7 the cloud layer, and that these more numerous rain drops produce larger evaporation rates at
8 both cloud top and cloud base. Examining the cloud and rainfall properties for the three
9 simulations, shows that for this stratocumulus case the parameterisation uncertainties for a
10 bulk scheme are larger than the effects of turbulence.

11 Comparing the simulations that use the turbulent and non-turbulent microphysics schemes of
12 Franklin, shows that the effects of turbulence on the droplet collision rates increases the
13 evaporation of rain water and leads to greater variability and higher TKE throughout both the
14 cloud and subcloud layers. The enhanced rain water in the turbulent microphysics simulation
15 has a weak positive feedback, with more rain producing more evaporation of drizzle drops at
16 cloud base, which destabilizes the subcloud layer and leads to stronger circulations and TKE
17 (Feingold et al. 1996). The observations for this case showed that the vertical winds were
18 negatively skewed just above cloud base (Ackerman et al. 2009) and the simulation with the
19 turbulent microphysics produces a closer match with nearly equal strength between updrafts
20 and downdrafts at this height (Fig. 9f).

21

22 **4 Sensitivity to cloud droplet number concentrations**

23 Four simulations of the stratocumulus and shallow convection cases were performed with
24 each of the non-turbulent and turbulent microphysics parameterisations. The simulations
25 differ in the prescribed CDNC and reveal how the cloud properties change with changes in
26 aerosol loading as manifested in changes of cloud droplet number. These simulations are not
27 designed to reflect the complete aerosol-cloud interactions but rather to provide some insights
28 into whether the effects of turbulence on cloud droplet interactions negate some of the
29 reduction in precipitation that tends to occur with increasing cloud droplet number
30 concentrations and the associated decrease in precipitation efficiency.

31 Figure 10 shows the average cloud properties over the last 4 hours of the RF02 simulations of
32 DYCOMS II, with the standard deviations shown by the bars. The cloud fraction increases

1 monotonically for both the non-turbulent and turbulent cases as the CDNC increases from 25
2 to 220 cm^{-3} . There is a strong relationship between increasing cloud fraction and decreasing
3 rain water path as the CDNC is increased. This result for a drizzling stratocumulus cloud
4 agrees with the conceptual model that greater aerosol loading and associated CDNC
5 suppresses precipitation formation and leads to larger cloud fractions (Albrecht 1989). For the
6 CDNC values explored here, the non-turbulent microphysics simulations demonstrate that
7 stratocumulus clouds typical of this case study increase the amount of cloud water and reduce
8 the rain water content when there is an increase in cloud droplet number, therefore, they show
9 a positive second aerosol indirect effect (Fig. 10b; Stevens et al. 1998). While this is also true
10 for the lowest three CDNC used in this study for the turbulent microphysics simulations, for
11 the highest concentration of $220 \text{ droplets cm}^{-3}$ the turbulent microphysics simulation shows a
12 reduction in both the rain and liquid water paths. The reduced rain water leading to a reduced
13 liquid water path in the turbulent microphysics simulation with highest CDNC shows a
14 negative second aerosol indirect effect. Other studies have also shown a non-monotonic
15 increase in LWP with increasing aerosol concentrations and suggest that there is a limit to the
16 degree of liquid water that can build up, with increasing efficiency of evaporation due to
17 larger concentrations of smaller drops likely playing a role (Xue et al. 2008). However, in this
18 case the variability of the liquid water paths is significantly larger than the small reduction in
19 liquid water path for the highest CDNC and, therefore, this is unlikely to be a robust physical
20 result for this simulation.

21 Figure 10c shows that there is an increase in the cloud base heights as cloud droplet numbers
22 are increased and precipitation is decreased. This has been found before, for example by
23 Savic-Jovicic and Stevens (2008), who showed that cloud base lowers in regions of
24 precipitation due to the precipitation changes affecting the thermodynamic state of the
25 subcloud layer. This can be seen through the tendency of the TKE to increase with CDNC in
26 all simulations except for the turbulent case with highest CDNC (Fig. 10d). An important
27 aspect for this work is that the TKE is greater for the turbulent microphysics simulations
28 compared to the corresponding non-turbulent simulation for each CDNC, except for the case
29 with the largest CDNC where the behaviour changes due to a reduction in liquid water path.
30 These results reflect the positive feedback that the turbulent microphysics parameterisations
31 have on increasing the TKE, which will then produce greater precipitation. However, these
32 results need to be interpreted with caution due to the large variability shown in the liquid
33 water path and TKE fields. Xue and Feingold (2006) studied the impact of increasing aerosol

1 concentrations on shallow cumuli cloud properties and found that the influence from aerosols
2 was less than the dynamical variability of the system in all fields examined except for the
3 cloud optical depths. This result is seen in Figure 10 where it can be seen that the variability
4 in all of the fields is large compared to the changes due to either the inclusion of turbulence
5 effects or the CDNC. The rain water path is the only field that shows a significant change in
6 rain water with changes in the CDNC. For this stratocumulus case the effects of turbulence on
7 rainfall are not statistically significant and instead it is the CDNC that has the largest control
8 on the rain water.

9 Figure 11 shows the effects of increasing the CDNC in the RICO simulations. In this shallow
10 cumulus convection case the liquid water path increases as the rain water path increases,
11 which is the opposite of the stratocumulus case. Increased CDNC results in reduced rainwater
12 in both cases, but in the RICO cases this also results in reduced liquid water paths. The
13 increased CDNC will tend to slow the collision-coalescence process, enhance evaporation and
14 reduce the drop fall speeds (Xue and Feingold 2006). The result of this and the subsequent
15 feedbacks in these small clouds is to reduce the liquid water path as well as the amount of
16 precipitation. Therefore, for this case all simulations produce a negative second aerosol
17 indirect effect, except for the highest CDNC using the non-turbulent microphysics scheme,
18 which shows a small increase in liquid water path. The change in average cloud fraction for
19 all simulations is small and generally less than 1%. As shown in Xue et al. (2008) this may be
20 due to the cancellation of changes in cloud size and cloud frequency.

21 The TKE response to increased CDNC in the shallow cumulus convection case is shown in
22 Figure 11b. Both sets of simulations tend to show an increase in vertically averaged TKE as
23 CDNC increases, with the largest changes occurring for the smallest CDNC in the turbulent
24 microphysics set and the highest CDNC in the non-turbulent set. The simulation that produces
25 the largest TKE is the non-turbulent microphysics scheme case with the highest CDNC. This
26 is due to a significant increase in the vertical velocity variance and buoyancy production of
27 TKE, which is responsible for the liquid water path being larger in this case than the
28 simulation with CDNC of 100 cm^{-3} . Examining the profiles of buoyancy production of TKE
29 for the non-turbulent microphysics cases, shows that the reduction in vertically integrated
30 TKE as CDNC reduces and rain water increases is due to the negative feedback that the
31 enhanced precipitation has on the buoyancy production of TKE, as discussed previously.
32 Figure 11 shows that the liquid water paths almost converge for the turbulent and non-

1 turbulent simulations with the largest CDNC due to the similar smaller rain water paths and
2 the reduced effect of the turbulence enhanced autoconversion and accretion rates.

3

4 **5 Summary**

5 Use of the bulk warm rain microphysics parameterisations of Franklin (2008) in the UCLA-
6 LES has allowed an investigation into the effects of turbulence on cloud droplet collision-
7 coalescence in stratocumulus and shallow convective clouds. The microphysics
8 parameterisations that include the effects of turbulence on droplet collision rates had a greater
9 impact on the simulated precipitation rates in the shallow convection case, where the larger
10 dissipation rates of TKE produced a more rapid conversion of cloud water to rain water. The
11 amount of rain water reaching the surface was 6 times larger in the simulation with the
12 turbulent microphysics scheme. The much weaker dissipation rates in the stratocumulus case,
13 however, also showed a change in the simulated precipitation when the effects of turbulence
14 on microphysical processes were included in the model, with rain water paths increasing by
15 17%. However, unlike the shallow convection case this is not a statistically significant result.

16 Both cases using the turbulent microphysics scheme produced greater evaporation rates of
17 rain water, which caused a change in the thermodynamics of the subcloud layer, destabilizing
18 the lower levels and enhancing the horizontal variability and TKE in this region. The
19 difference in the precipitation-dynamical feedbacks between the two cases was in the upper
20 levels of the clouds where the liquid water contents are largest. In the shallow convection case
21 the greater rain and cloud water loading and enhanced latent heating associated with the larger
22 liquid water in the turbulent microphysics simulation, reduced the buoyancy production of
23 TKE and the entrainment. Therefore, in this case a negative precipitation-dynamical feedback
24 to the enhanced precipitation formation associated with turbulent microphysics effects was
25 produced. In contrast, the stratocumulus case showed a weak positive feedback, with
26 enhanced rainwater and rain water evaporation in the simulation with the turbulent
27 microphysical parameterisations producing greater TKE in both the subcloud layer and in the
28 upper cloud region. Including the results from the other bulk microphysics schemes (Seifert
29 and Beheng for the RICO case and Khairoutdinov and Kogan for the DYCOMSII case)
30 demonstrated that including the effects of turbulence on droplet collision rates had a larger
31 impact than the different microphysics scheme for the shallow convection case, but that the
32 opposite is true for the stratocumulus case. These results highlight the significant

1 parameterisation uncertainties associated with bulk schemes in their simulations of
2 stratocumulus clouds.

3 Sensitivity studies where the CDNC was varied showed agreement with the conceptual model
4 for lightly drizzling stratocumulus clouds, that greater CDNC suppresses precipitation
5 formation leading to larger cloud fraction and liquid water paths (Albrecht 1989). This can be
6 interpreted as a positive second indirect aerosol effect, and was produced in all of the
7 DYCOMS II simulations except for the case using the turbulent microphysics with the highest
8 CDNC which showed a small reduction in liquid water path. The RICO shallow convection
9 case produced a negative second indirect aerosol effect in all but one simulation. The
10 increased CDNC in the small convective clouds reduced the production of rainwater,
11 enhanced the evaporation and led to a reduction in the liquid water path. While the sign of the
12 second indirect effect is negative in the shallow convection case whether the effects of
13 turbulence on cloud droplet collisions are considered or not, the magnitude of the effect is
14 doubled when the turbulent microphysics are used. Liquid water paths reduce from 19.1 to
15 16.1 g m⁻² for the non-turbulent microphysics simulations as CDNC increases from 40 to 200
16 cm⁻³, whereas for the turbulent microphysics simulations the liquid water paths change from
17 24.2 to 16.7 g m⁻².

18 The results presented in this work are by no means a definitive or quantitative statement as to
19 how the effects of turbulence on cloud collision and coalescence impacts precipitation and
20 cloud properties. Larger domains and higher resolution simulations need to be conducted in
21 the future to test how robust the features are that have been described in this study. Seifert et
22 al. (2010) performed a set of simulations at double the horizontal resolution of their control
23 case and found a reduction in the rainfall increase due to turbulent enhancement. How this
24 may change with further refinement of the computational grid remains to be seen. Matheou et
25 al. (2011) found that the negative buoyancy zones that occur at the cloud-environment
26 interface are unresolved for typical LES resolutions and discussed the impact that this may
27 have on modelling the entrainment process. Higher resolution simulations that better resolve
28 entrainment could show a change in the buoyancy and entrainment results found in this study.
29 In addition, other case studies and thermodynamic profiles should be tested to investigate the
30 sensitivity of the effects to changes in the large scale environment. Refinements and further
31 developments to the turbulent collision kernels and collision efficiencies are also required to
32 advance the knowledge regarding the effects of turbulence on cloud microphysics, the

1 formation of precipitation and the precipitation-dynamical feedbacks. Wyszogrodzki et al.
2 (2013) describe their aims of developing an integrated multiscale computational approach that
3 combines LES and direct numerical simulations approaches. This would provide a unique
4 way to simulate the wide range of scales involved with precipitation formation from
5 kilometres to millimetres.

6 As discussed by Savic-Jovicic and Stevens (2008), often LES require lower CDNC than
7 observed to initiate precipitation, and this includes both bulk and bin models. Including the
8 effects of turbulence in the microphysics parameterisations minimizes this need to artificially
9 reduce CDNC in order to simulate observed precipitation rates. How much of this effect may
10 be due to a better physical representation of the collision process or to numerical limitations is
11 an open question. Use of observations to try to answer this would be a worthwhile endeavour;
12 however, as noted by Xue and Feingold (2006), the variability of the cloud fields in shallow
13 convection simulations where the impact of the turbulence enhancement is largest might make
14 this somewhat challenging. For example, the changes to liquid water paths due to the effects
15 of turbulent microphysics are much smaller than the standard deviations of the liquid water
16 path of any given simulation by about an order of magnitude. In this study the analysis of the
17 turbulent enhancement and the precipitation-dynamical feedbacks has been on a scale larger
18 than that of an individual cloud. Future work will investigate individual cloud properties and
19 life cycles to examine the effects that the microphysics parameterisations that include the
20 effects of turbulence may have on the cloud scale.

21

22 **Acknowledgements**

23 This research is funded by the Australian Government Department of the Environment, the
24 Bureau of Meteorology and CSIRO through the Australian Climate Change Science Program.
25 Bjorn Stevens from the Max Planck Institute for Meteorology is thanked for providing the
26 UCLA LES model code. Three anonymous reviewers are thanked for providing insightful and
27 constructive comments that helped to improve the manuscript.

28

1 **References**

- 2 Ackerman, A.S., vanZanten, M.C., Stevens, B., Savic-Jovicic, V., Bretherton, C.S., Chlond,
3 A., Golaz, J.-C., Jiang, H., Khairoutdinov, M., Krueger, S.K., Lewellen, D.C., Lock, A.,
4 Moeng, C.-H., Nakamura, K., Petters, M.D., Snider, J.R., Weinbrecht, S. and Zuluaf, 2009:
5 Large-eddy simulations of a drizzling, stratocumulus-topped marine boundary layer. *Mon.*
6 *Wea. Rev.*, 137, 1083-1110
- 7 Albrecht, B.A., 1989: Aerosols, cloud microphysics, and fractional cloudiness. *Science*, 245,
8 1227-1230
- 9 Ayala, O., B. Rosa, L.-P. Wang and W. Grabowksi, 2008: Effects of turbulence on the
10 geometric collision rate of sedimenting droplets. Part 2. Theory and parameterization. *New J.*
11 *Phys.*, doi:10.1088/1367-2630/10/075016
- 12 Beard, K.V. and H.T. Ochs, 1993: Warm-rain initiation: An overview of microphysical
13 mechanisms. *J. Appl. Meteor.*, 32, 608-625
- 14 Feingold, G., W.R. Cotton, B. Stevens and S.A. Frisch, 1996: The relationship between in-
15 cloud residence time and drizzle production in numerically simulated stratocumulus clouds. *J.*
16 *Atmos. Sci.*, 53, 1108-1122
- 17 Franklin, C.N., P.A. Vaillancourt, M.K. Yau, and P. Bartello, 2005: Collision rates of cloud
18 droplets in turbulent flow. *J. Atmos. Sci.*, 62, 2451-2466
- 19 Franklin, C.N., P.A. Vaillancourt, and M.K. Yau, 2007: Statistics and parameterisations of the
20 effect of turbulence on the geometric collision kernel of cloud droplets. *J. Atmos. Sci.*, 64,
21 938-945
- 22 Franklin, C.N., 2008: A warm rain microphysics parameterisation that includes the effects of
23 turbulence. *J. Atmos. Sci.*, 65, 1795-1816
- 24 Grabowski, W.W. and L.-P. Wang, 2013: Growth of cloud droplets in a turbulent
25 environment. *Ann. Rev. Fluid Mechanics*, 45, 293-324
- 26 Jiang, H. and W.R. Cotton, 2000: Large eddy simulation of shallow cumulus convection
27 during BOMEX: Sensitivity to microphysics and radiation. *J. Atmos. Sci.*, 57, 582-594
- 28 Khairoutdinov, M. and Y. Kogan, 2000: A new cloud physics parameterisation in a large-
29 eddy simulation model of marine stratocumulus. *J. Atmos. Sci.*, 57, 229-243

1 Kunnen, R.P.J., C. Siewert, M. Meinke, W. Schröder and K.D. Beheng, 2013: Numerically
2 determined geometric collision kernels in spatially evolving isotropic turbulence relevant for
3 droplets in clouds. *Atmos. Res.*, 127, 8-21

4 Matheou, G., D. Chung, L. Nuijens, B. Stevens and J. Teixeira, 2011: On the fidelity of large-
5 eddy simulation of shallow precipitating cumulus convection. *Mon. Wea. Rev.*, 139, 2918-
6 2939

7 Pinsky, M.B., A.P. Khain, B. Grits and M. Shapiro, 2006: Collisions of small drops in a
8 turbulent flow. Part III: Relative droplet fluxes and swept volumes. *J. Atmos. Sci.*, 63, 2123-
9 2139

10 Rauber, R.M., Ochs, H.T., Di Girolamo, L., Göke, S., Snodgrass, E., Stevens, B., Knight, C.,
11 Jensen, J.B., Lenschow, D.H., Rilling, R.A., Rogers, D.C., Stith, J.L., Albrecht, B.A.,
12 Zuidema, P., Blyth, A.M., Fairall, C.W., Brewer, W.A., Tucker, S., Lasher-Trapp, S.G.,
13 Mayol-Bracero, O.L., Vali, G., Geerts, B., Anderson, J.R., Baker, B.A., Lawson, R.P., Bandy,
14 A.R., Thornton, D.C., Burnet, E., Brenguier, J.-L., Gomes, L., Brown, P.R.A., Chuang, P.,
15 Cotton, W.R., Gerber, H., Heikes, B.G., Hudson, J.G., Kollias, P., Krueger, S.K., Nuijens, L.,
16 O'Sullivan, D.W., Siebesma, A.P. and Twohy, C.H., 2007: Rain in (shallow) cumulus over the
17 ocean – the RICO campaign. *Bull. Amer. Meteor. Soc.*, 88, 1912-1928

18 Savij-Jovicic, V. and B. Stevens, 2008: The structure and organization of precipitating
19 stratocumulus. *J. Atmos. Sci.*, 65, 1587-1605

20 Seifert, A., and K.D. Beheng, 2001: A double-moment parameterisation for simulating
21 autoconversion, accretion and self collection. *Atmos. Res.*, 59-60, 265-281

22 Seifert, A., and T. Heus. 2013: Large-eddy simulation of organized precipitating trade wind
23 cumulus clouds. *Atmos. Chem. Phys.*, 13, 5631-5645

24 Seifert, A., L. Nuijens and B. Stevens, 2010: Turbulence effects on warm-rain autoconversion
25 in precipitating shallow convection. *Q. J. R. Meteor. Soc.*, 136, 1753-1762

26 Siebesma, A.P., C.S. Bretherton, A. Brown, A. Chlond, J. Cuxart, P.G. Duynkerke, H. Jiang,
27 M. Khairoutdinov, D. Lewellen, C.-H. Moeng, E. Sanchez, B. Stevens and D.E. Stevens,
28 2003: A large eddy simulation intercomparison study of shallow cumulus convection. *J.*
29 *Atmos. Sci.*, 60, 1201-1219

1 Stevens, B., W.R. Cotton, G. Feingold and C.-H. Moeng, 1998: Large-eddy simulations of
2 strongly precipitating, shallow, stratocumulus-topped boundary layers. *J. Atmos. Sci.*, 55,
3 3963-3984

4 Stevens, B., Ackerman, A.S., Albrecht, B.A., Brown, A.R., Chlond, A., Cuxart, J.,
5 Duynkerke, P.G., Lewellen, D.C., Macvean, M.K., Neggers, R.A.J., Sánchez, E., Siebesma,
6 A.P. and Stevens, D.E., 2001: Simulations of trade-wind cumuli under a strong inversion. *J.*
7 *Atmos. Sci.*, 58, 1870-1891

8 Stevens, B., Moeng, C.-H., Ackerman, A.S., Bretherton, C.S., Chlond, A., de Roode, S.,
9 Edwards, J., Golaz, J.-C., Jiang, H., Khairoutdinov, M., Kirkpatrick, M.P., Lewellen, D.C.,
10 Lock, A., Müller, F., Stevens, D.E., Whelan, E., and Zhu, 2005: Evaluation of large-eddy
11 simulations via observations of nocturnal marine stratocumulus. *Mon. Wea. Rev.*, 133, 1443-
12 1462

13 Stevens, B., 2007: On the growth of layers of non-precipitating cumulus convection. *J. Atmos.*
14 *Sci.*, 64, 2916-2931

15 vanZanten, M.C. and B. Stevens, 2005: Observations of the structure of heavily precipitating
16 marine stratocumulus. *J. Atmos. Sci.*, 62, 4327-4342

17 vanZanten, M.C., Stevens, B., Nuijens, L., Siebesma, A.P., Ackerman, A.S., Burnet, F.,
18 Cheng, A., Couvreux, F., Jiang, H., Khairoutdinov, M., Kogan, Y., Lewellen, D.C., Mechem,
19 D., Nakamura, K., Noda, A., Shipway, B.J., Slawinska, J., Wang, S. and Wyszogrodzki, A.,
20 2011: Controls on precipitation and cloudiness in simulations of trade-wind cumulus as
21 observed during RICO. *J. Adv. Model. Earth Syst.*, 3, M06001, doi: 10.1029/2011MS000056

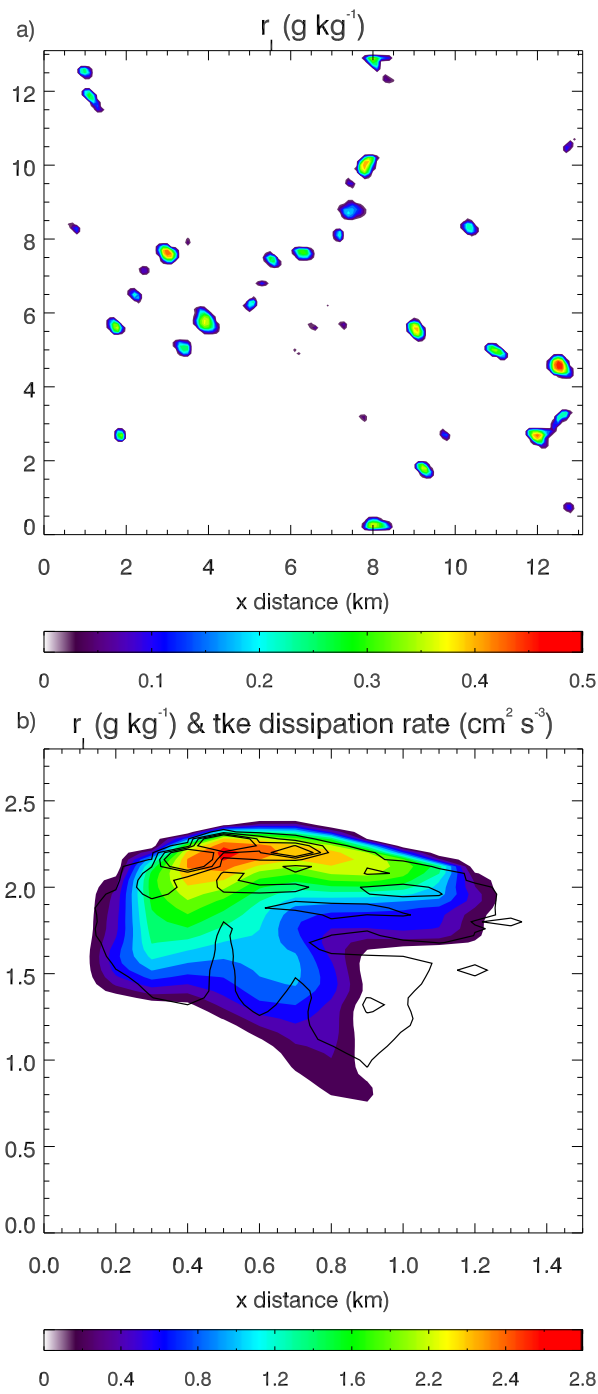
22 Wang, L.-P. and M.R. Maxey, 1993: Settling velocity and concentration distribution of heavy
23 particles in homogeneous isotropic turbulence. *J. Fluid Mech.*, 256, 27-68

24 Wang, L.-P., O. Ayala, S.E. Kasprzak and W.W. Grabowski, 2005: Theoretical formulation
25 of collision rate and collision efficiency of hydrodynamically-interacting cloud droplets in
26 turbulent atmosphere. *J. Atmos. Sci.*, 62, 2433-2450

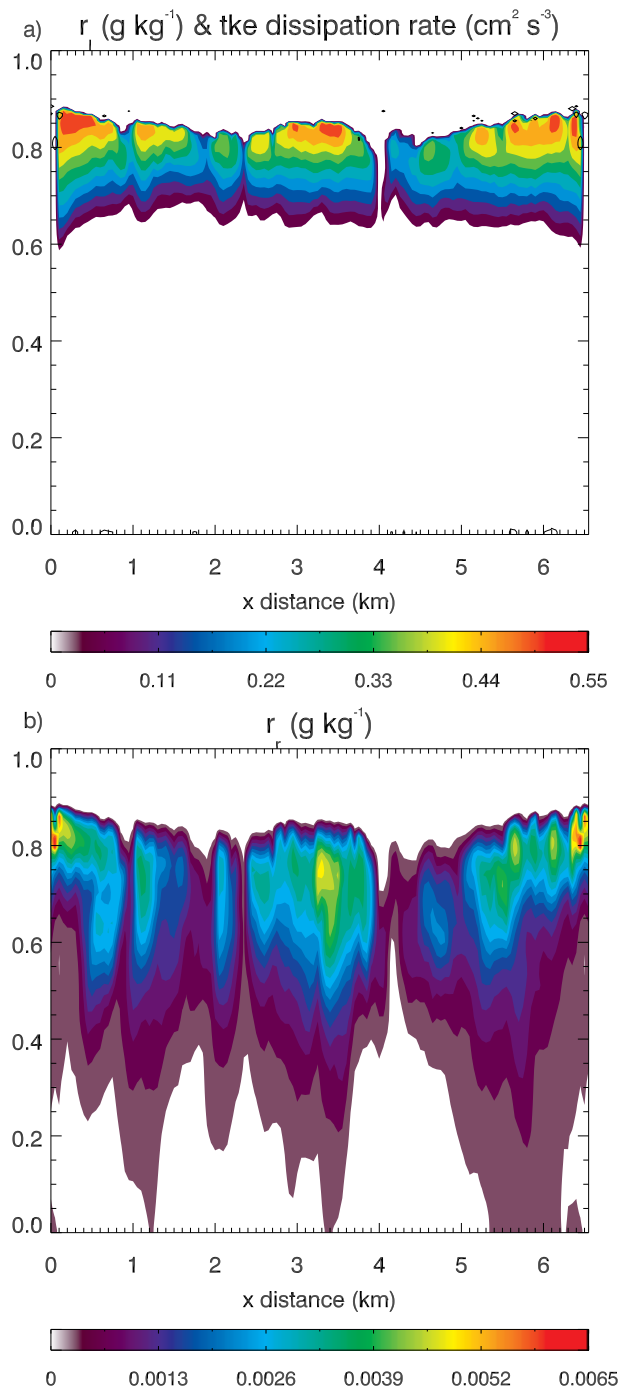
27 Wang, L.-P., O. Ayala, B. Rosa and W.W. Grabowski, 2008: Turbulent collision efficiency of
28 heavy particles relevant to cloud droplets. *New J. Phys.*, 62: 2433-2450

29 Wang, Y., J. Fan, R. Zhang, L.R. Leung and C. Franklin, 2013: Improving bulk microphysics
30 parameterizations in simulations of aerosol effects. *J. Geophys. Res.*, 118, 5361-5379

- 1 Wyszogrodzki, A.A., W.W. Grabowski, L.-P. Wang and O. Ayala, 2013: Turbulent collision-
2 coalescence in maritime shallow convection. *Atmos. Chem. Phys. Discuss.*, 13, 8471–8487,
3 doi:10.5194/acp-13-8471-2013
- 4 Xue, H. and G. Feingold, 2006: Large-eddy simulations of trade wind cumuli: Investigation
5 of aerosol indirect effects. *J. Atmos. Sci.*, 63, 1605-1622
- 6 Xue, H., G. Feingold and B. Stevens, 2008: Aerosol effects on clouds, precipitation, and the
7 organization of shallow cumulus convection. *J. Atmos. Sci.*, 65, 392-406
- 8
- 9

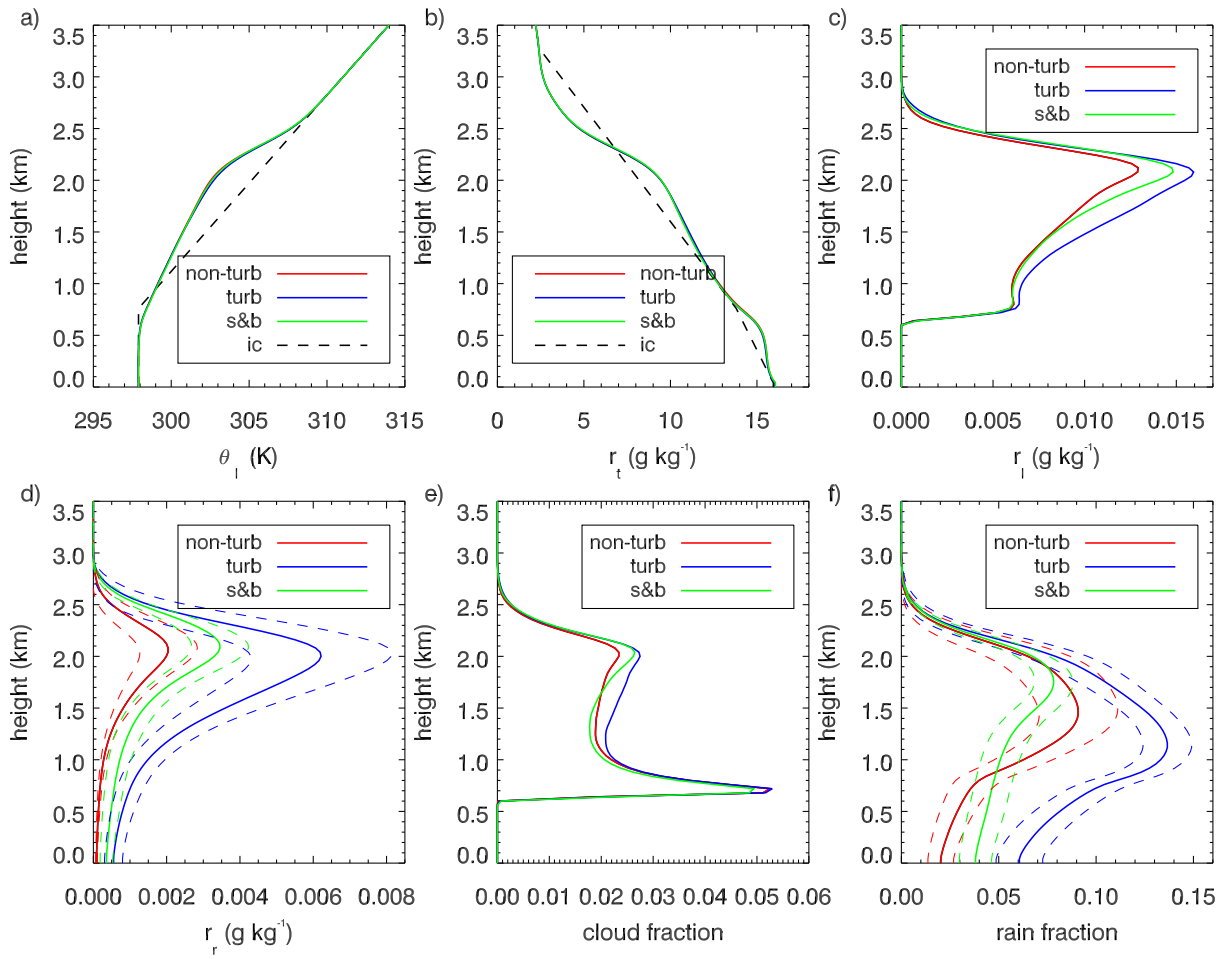


1
 2 Figure 1. a) Plan view of RICO liquid water mixing ratio (g kg^{-1}) at 840 m and b) cross-
 3 section through a typical cloud showing liquid water mixing ratio (g kg^{-1}) and contour lines of
 4 the dissipation rate of turbulent kinetic energy (contour levels are 100, 500, 1000, 1500 $\text{cm}^2 \text{s}^{-3}$).
 5
 6



1
 2 Figure 2. Cross sections of the a) liquid and b) rain water mixing ratios (g kg^{-1}) for the
 3 DYCOMS II case. Contour lines of the turbulent kinetic energy dissipation rate in a) are 100
 4 $\text{cm}^2 \text{s}^{-3}$.

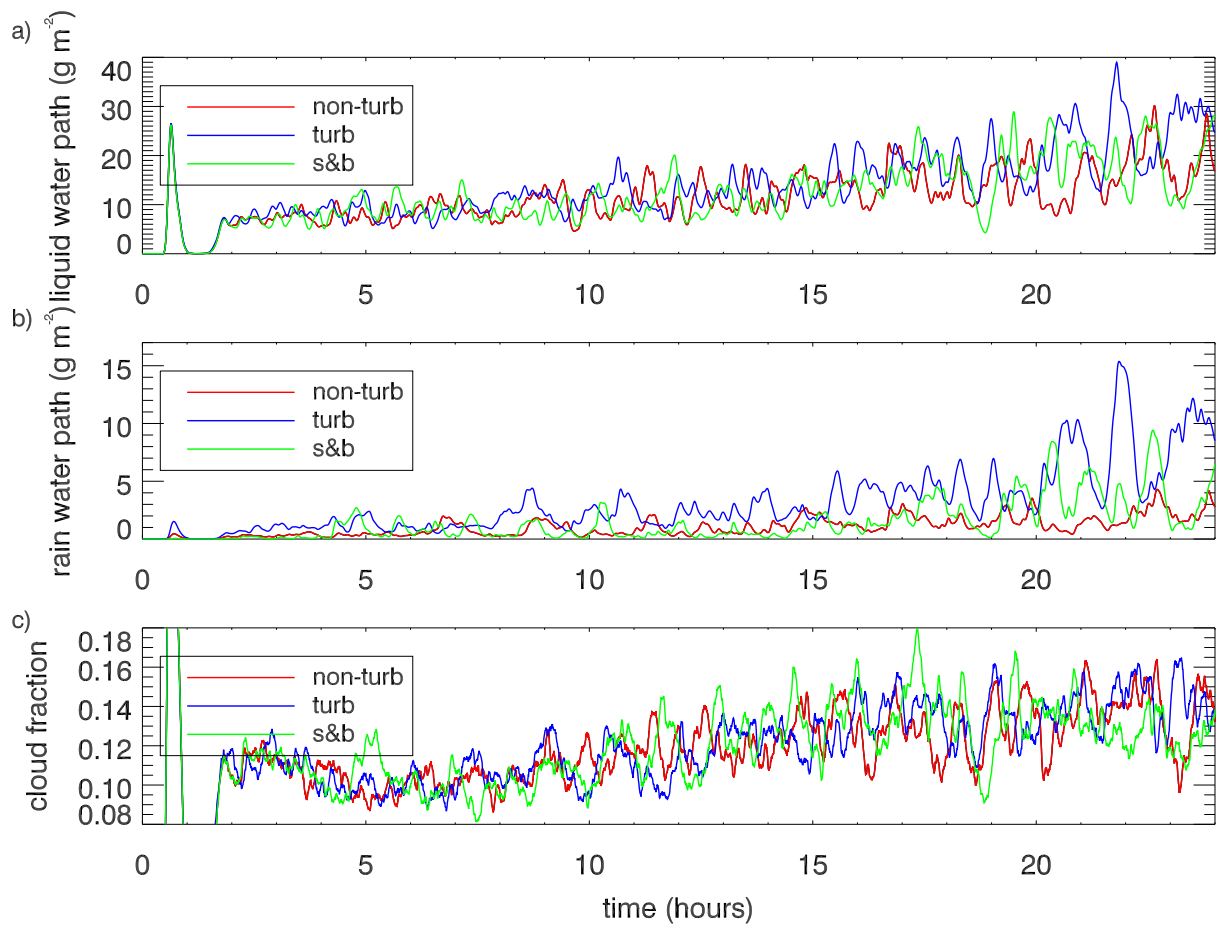
1



2

3 Figure 3. RICO cloud properties for the simulations that use the turbulent (blue) and non-
 4 turbulent (red) microphysics parameterisations of Franklin (2008) and the microphysics
 5 scheme of Seifert and Beheng (2001; green). The initial conditions are given by the black
 6 dashed lines. a) Liquid water potential temperature (K), b) total water mixing ratio (g kg^{-1}), c)
 7 liquid water mixing ratio (g kg^{-1}), d) rain water mixing ratio (g kg^{-1}), e) cloud fraction and f)
 8 rain fraction. The coloured dashed lines in d) and f) represent the \pm standard deviation from
 9 the temporal means, with these fields being the only ones that show significantly different
 10 means.

11

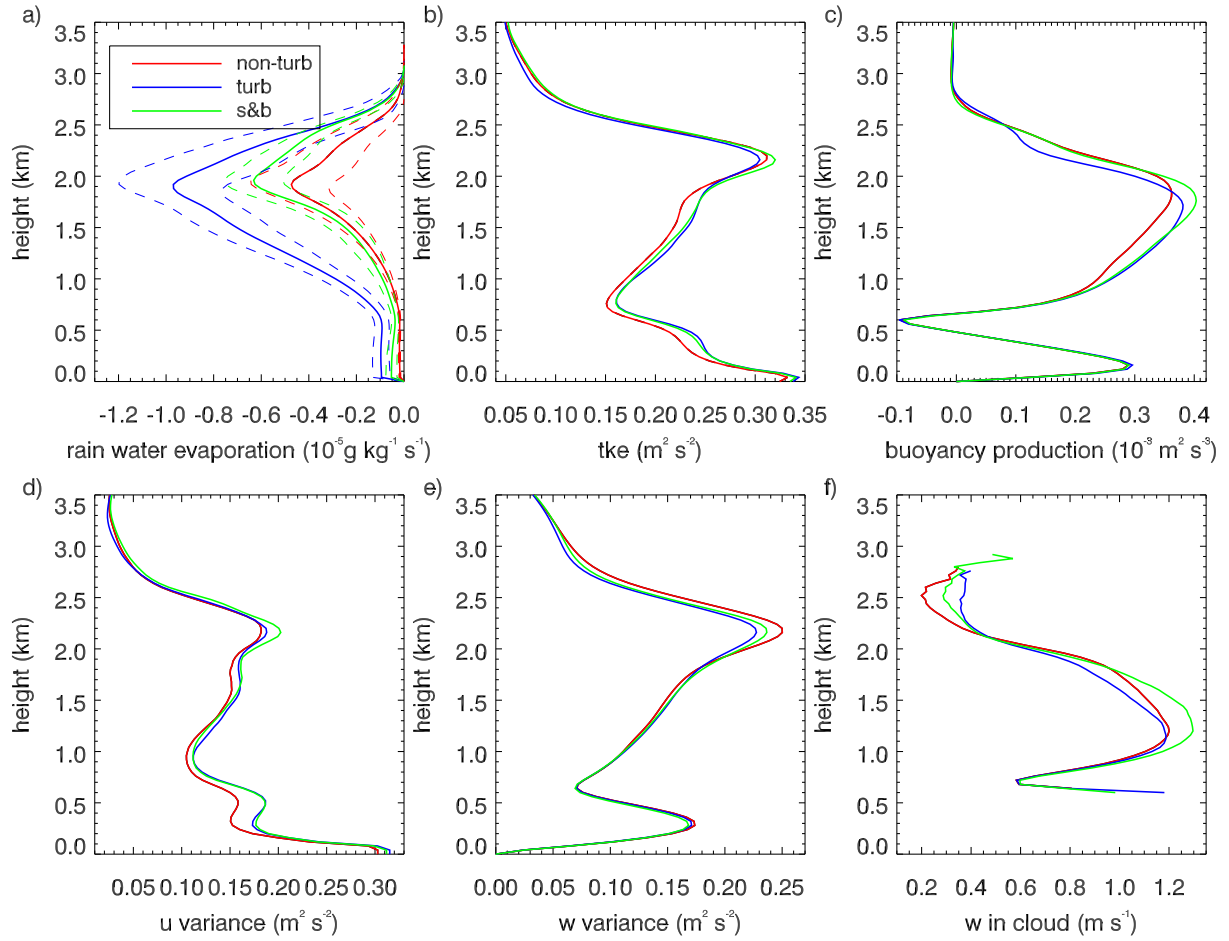


1

2

3 Figure 4. Time series of RICO a) liquid (cloud and rain) water path (g m^{-2}), b) rain water path
 4 (g m^{-2}) and c) cloud fraction for the simulations that use the turbulent (blue) and non-turbulent
 5 (red) microphysics parameterisations of Franklin (2008) and the microphysics scheme of
 6 Seifert and Beheng (2001; green).

1

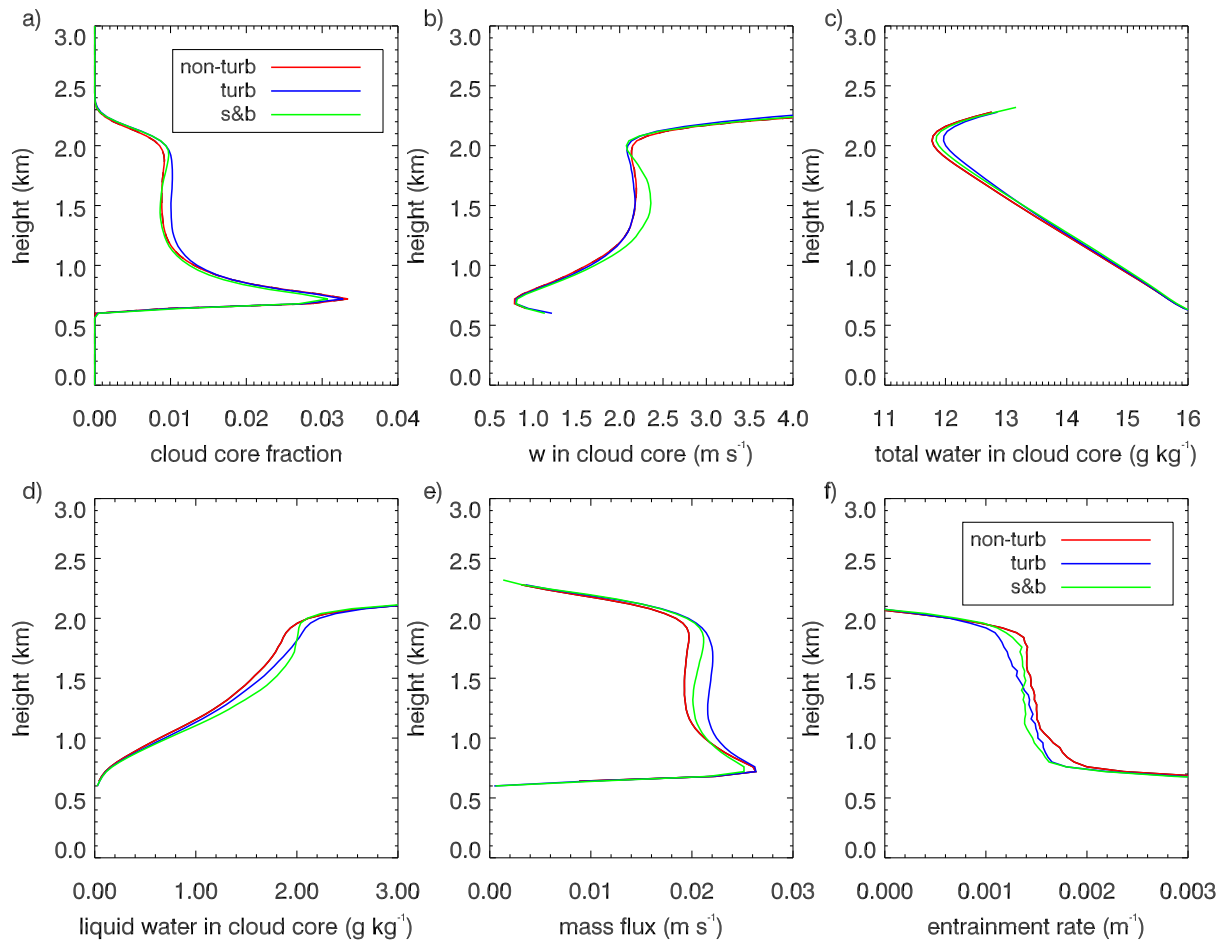


2

3 Figure 5. As in Fig. 3 except for, a) rain water evaporation ($\text{g kg}^{-1} \text{s}^{-1}$), b) turbulent kinetic
 4 energy ($\text{m}^2 \text{s}^{-2}$), c) resolved buoyancy production of turbulent kinetic energy ($10^{-4} \text{m}^2 \text{s}^{-3}$), d)
 5 variance of u component of horizontal wind ($\text{m}^2 \text{s}^{-2}$), e) variance of vertical velocity ($\text{m}^2 \text{s}^{-2}$)
 6 and f) conditional average of vertical velocity inside clouds (m s^{-1}). The coloured dashed lines
 7 in a) represent the \pm standard deviation from the temporal means, with the rain water
 8 evaporation being the only fields that show significantly different means.

9

10



1

2

3

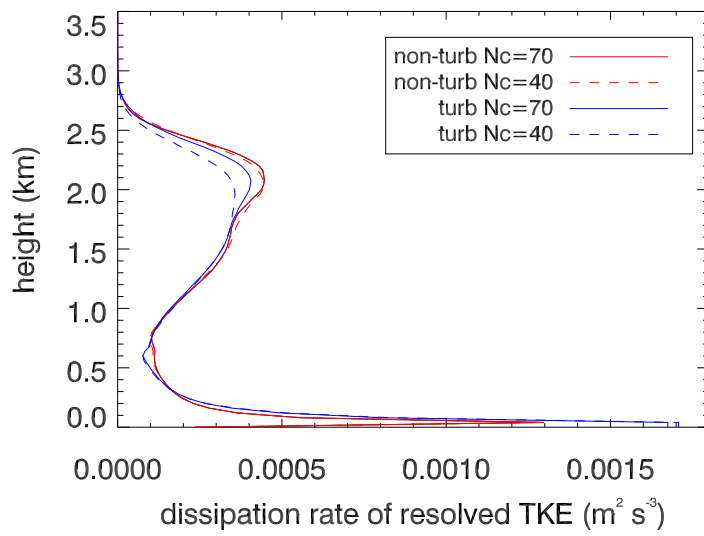
4

5

6

Figure 6. As in Fig. 3 except for, a) cloud core fraction, b) conditional average of vertical velocity inside cloud cores (m s^{-1}), c) conditional average of total water inside cloud cores (g kg^{-1}), d) conditional average of cloud liquid water in cloud cores (g kg^{-1}), e) mass flux (m s^{-1}), and f) entrainment rate (m^{-1}).

1

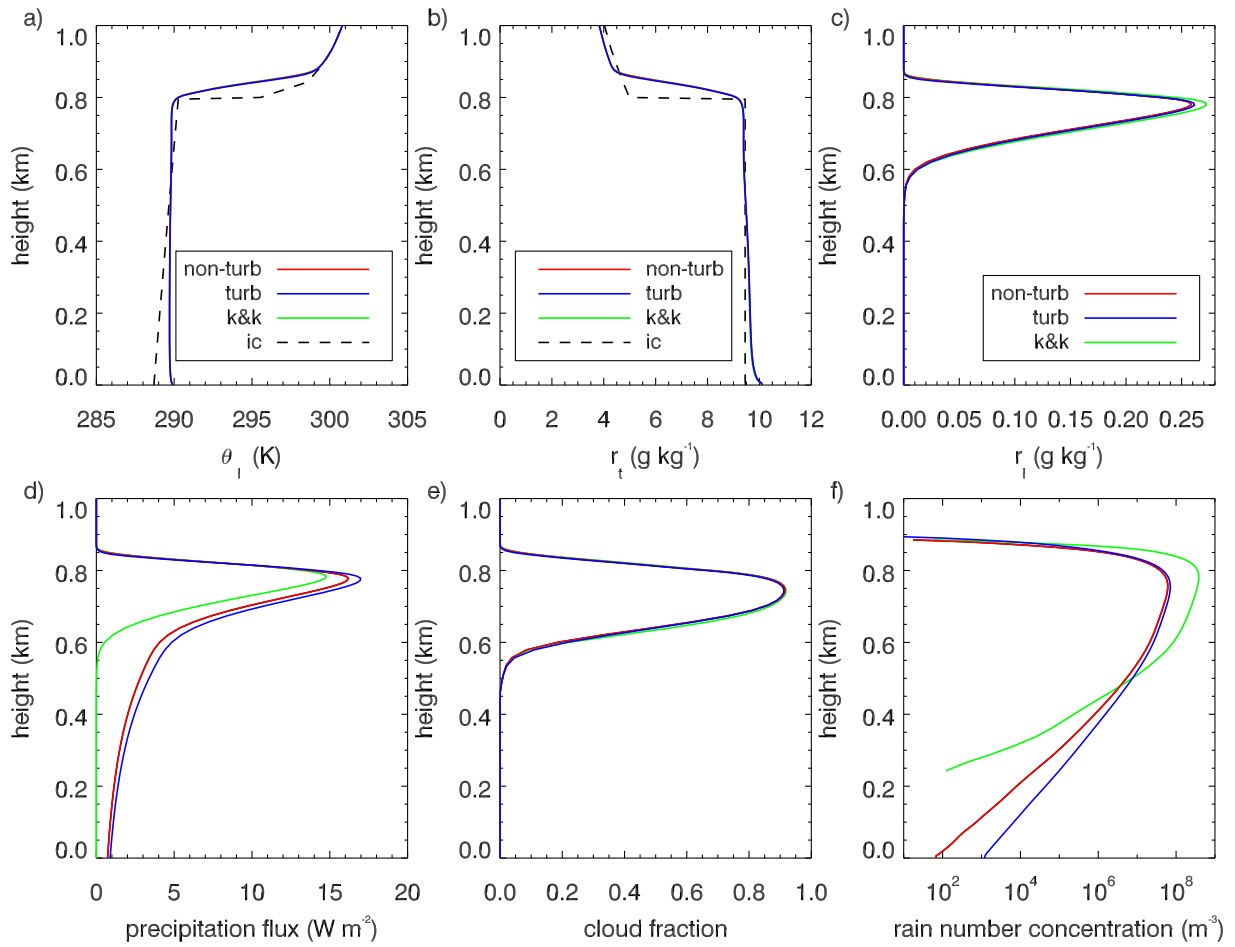


2

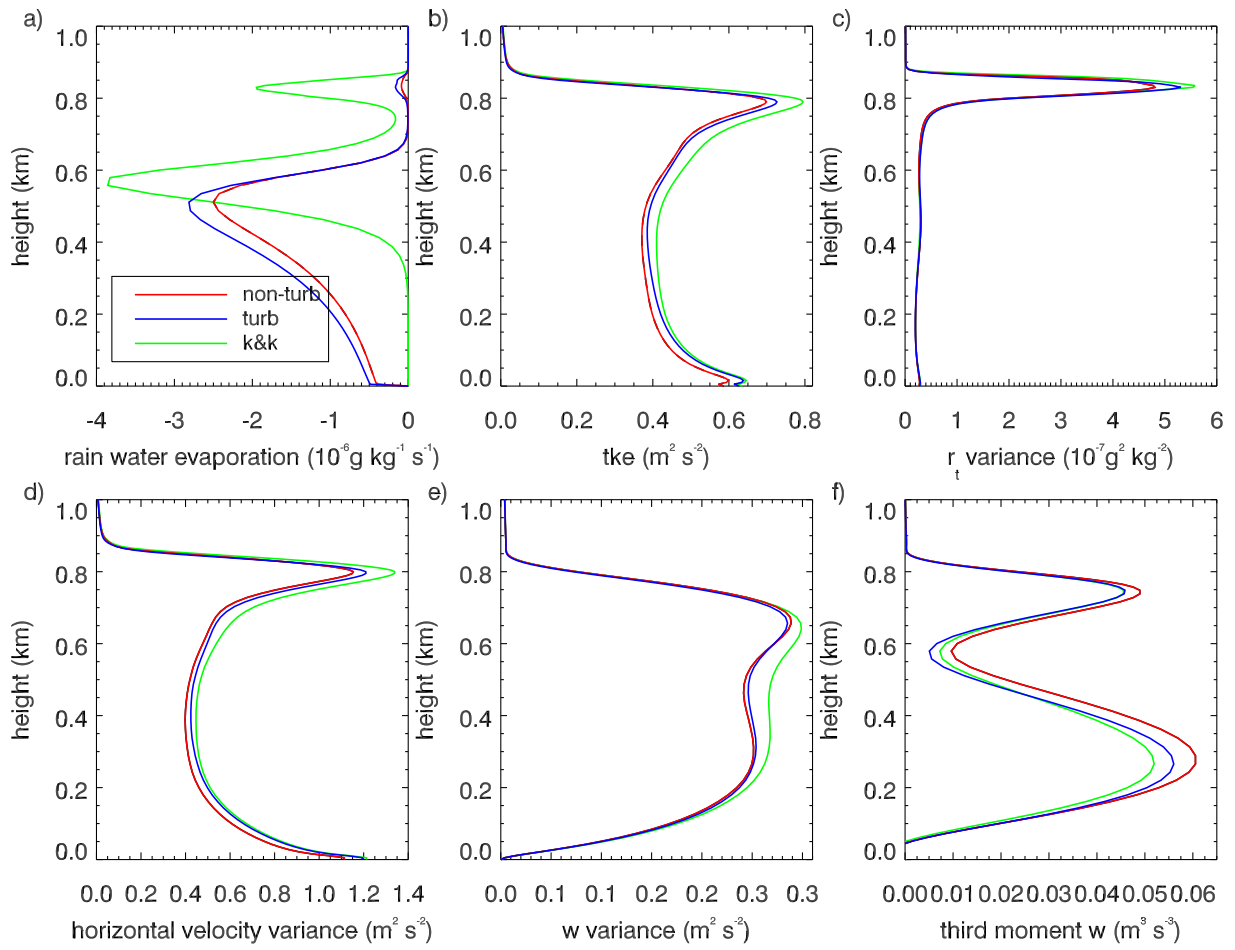
3

4 Figure 7. Dissipation rate of resolved TKE ($\text{m}^2 \text{s}^{-3}$) for the non-turbulent and turbulent
5 microphysics simulations for the control ($N_c = 70$) and a reduced cloud droplet number
6 concentration of $N_c = 40 \text{ cm}^{-3}$

7

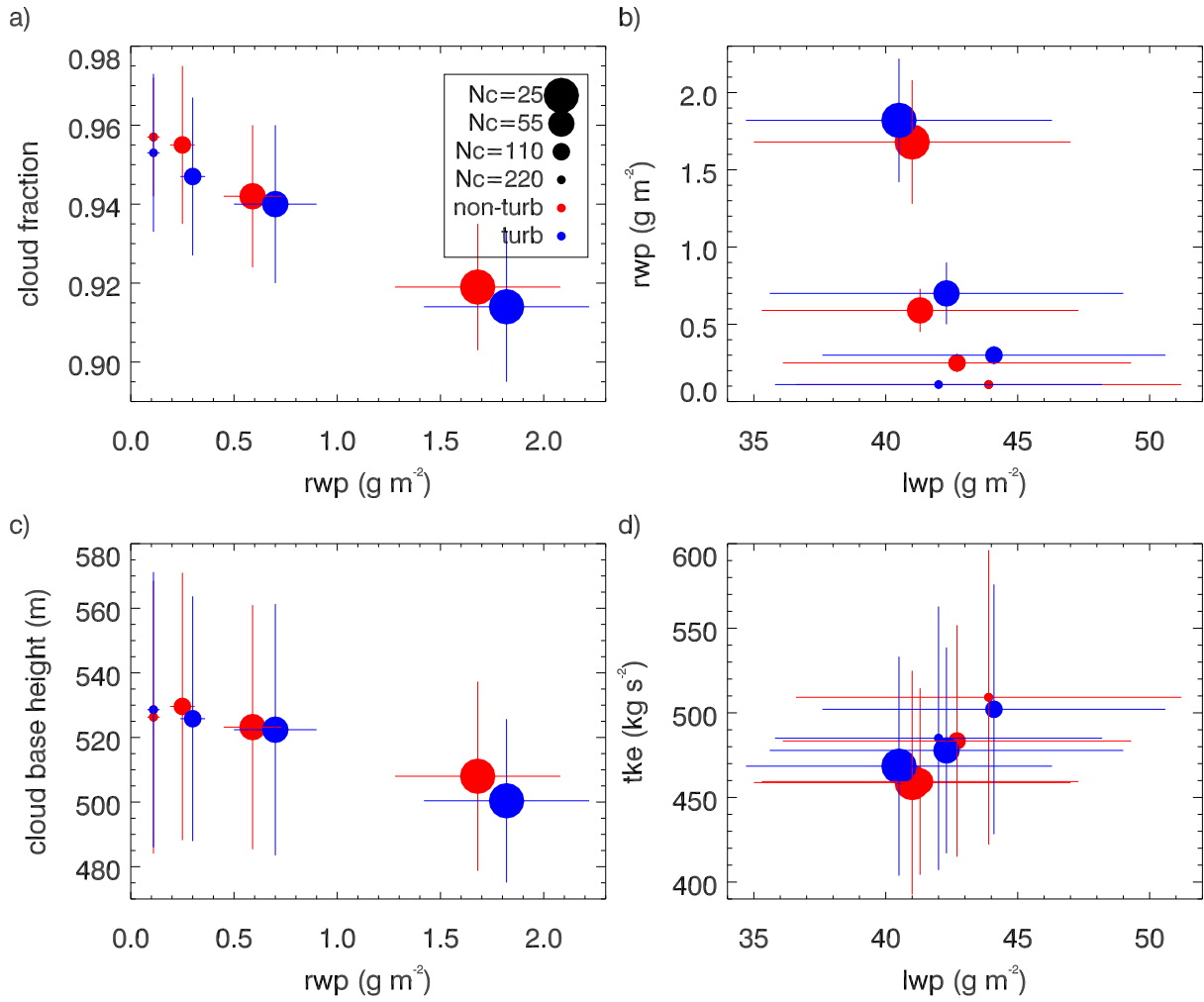


1
2 Figure 8. DYCOMS II cloud and dynamical properties for the simulations that use the turbulent
3 (blue) and non-turbulent (red) microphysics parameterisations of Franklin (2008) and the
4 microphysics scheme of Khairoutdinov and Kogan (2000; green). The initial conditions are
5 represented by the black dashed line. a) Liquid water potential temperature (K), b) total water
6 mixing ratio (g kg^{-1}), c) liquid water mixing ratio (g kg^{-1}), d) precipitation flux (W m^{-2}), e) cloud
7 fraction and f) rain drop number concentration (m^{-3}).
8



1
 2 Figure 9. As in Fig. 6 expect for, a) Rain water evaporation ($\text{g kg}^{-1} \text{s}^{-1}$), b) turbulent kinetic
 3 energy ($\text{m}^2 \text{s}^{-2}$), c) variance of liquid water ($\text{g}^2 \text{kg}^{-2}$), d) variance of horizontal velocity ($\text{m}^2 \text{s}^{-2}$), e)
 4 variance of vertical velocity ($\text{m}^2 \text{s}^{-2}$) and f) third moment of vertical velocity ($\text{m}^3 \text{s}^{-3}$).

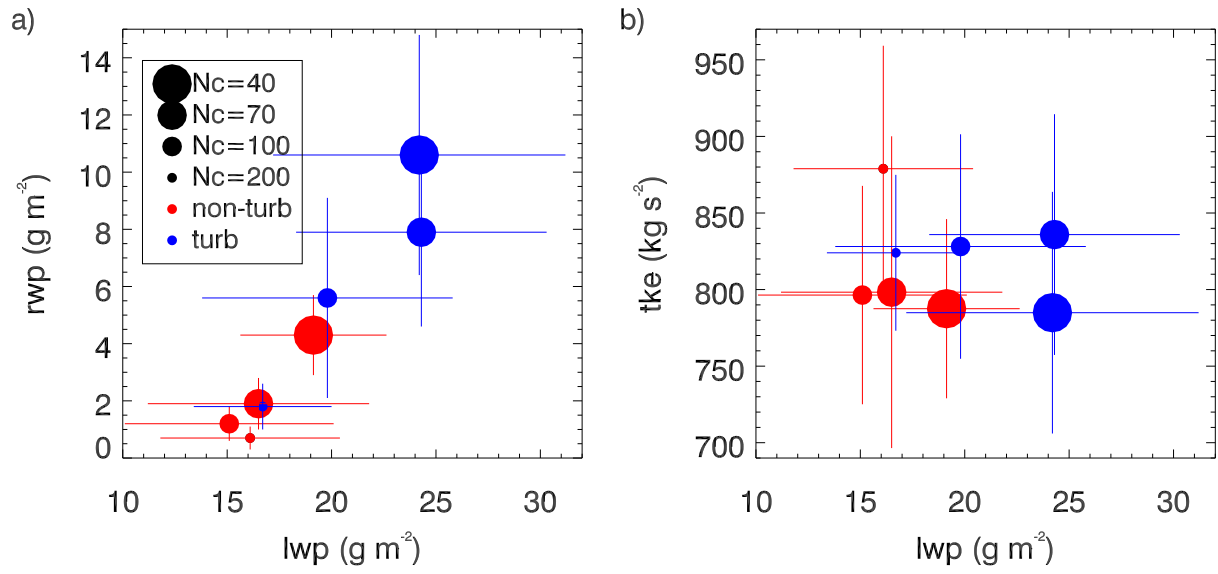
1



2

3 Figure 10. Average DYCOMS II cloud and dynamical properties for specified CDNC. Rain
 4 water path (g m⁻²) and a) cloud fraction and c) cloud base height (m). Liquid water path (g m⁻²)
 5 and b) rain water path (g m⁻²) and d) vertically integrated turbulent kinetic energy (kg s⁻²).
 6 The length of the bars denote the +/- standard deviations about the mean.

1



2

3 Figure 11. Average RICO cloud and dynamical properties for specified CDNC. Liquid water
4 path (g m^{-2}) and a) rain water path (g m^{-2}), and b) vertically integrated turbulent kinetic energy
5 (kg s^{-2}). The length of the bars denote the +/- standard deviations about the mean.

6